Mutational Analysis of the Active Site Flap (20s Loop) of Mandelate Racemase†

Jennifer R. Bourque and Stephen L. Bearne*

Department of Biochemistry and Molecular Biology, Dalhousie University, Halifax, Nova Scotia B3H 1X5, Canada

Received August 3, 2007; Revised Manuscript Received November 6, 2007

ABSTRACT: Mandelate racemase from *Pseudomonas putida* catalyzes the Mg^{2+}-dependent 1,1-proton transfer that interconverts the enantiomers of mandelate. Residues of the 20s and 50s loops determine, in part, the topology and polarity of the active site and hence the substrate specificity. Previously, we proposed that, during racemization, the phenyl ring of mandelate moves between an *S*-pocket comprised of residues from the 50s loop and an *R*-pocket comprised of residues from the 20s loop [Siddiqi, F., Bourque, J. R., Jiang, H., Gardner, M., St. Maurice, M., Blouin, C., and Bearne, S. L. (2005) *Biochemistry 44*, 9013−9021]. The 20s loop constitutes a mobile β-meander flap that covers the active site cavity shielding it from solvent and controlling entry and egress of ligands. To understand the role of the 20s loop in catalysis and substrate specificity, we constructed a series of mutants (V22A, V22I, V22F, T24S, A25V, V26A, V26L, V26F, V29A, V29L, V29F, V26A/V29L, and V22I/V29L) in which the sizes of hydrophobic side chains of the loop residues were varied. Catalytic efficiencies (k_{cat}/K_m) for all mutants were reduced between 6- and 40-fold with the exception of those of V22I, V26A, V29L, and V22I/V29L which had near wild-type efficiencies with mandelate. Thr 24 and Ala 25, located at the tip of the 20s loop, were particularly sensitive to minor alterations in the size of their hydrophobic side chains; however, most mutations were tolerated quite well, suggesting that flap mobility could compensate for increases in the steric bulk of hydrophobic side chains. With the exception of V29L, with mandelate as the substrate, and V22F and V26A/V29L, with 2-naphthylglycolate (2-NG) as the substrate, the values of k_{cat} and K_m were not altered in a manner consistent with steric obstruction of the *R*-pocket, perhaps due to flap mobility compensating for the increased size of the hydrophobic side chains. Surprisingly, V22I and V29L catalyzed the racemization of the bulkier substrate 2-NG with k_{cat}/K_m values ∼2-fold greater than those observed for wild-type mandelate racemase. Although minor changes in substrate specificity were achieved through alterations of the active site flap of mandelate racemase, our results suggest that hydrophobic residues that reside on a flexible flap and define the topology of an active site through their van der Waals contacts with the substrate are quite tolerant of a variety of steric substitutions.

Many enzymes possess a flexible loop, or "flap", that protrudes into bulk solvent in the unliganded enzyme and closes over the active site when ligand is bound. Such flaps may not only govern the rates of substrate binding and product release but also serve other important functions, including exclusion of water from the active site and modification of the dielectric environment of the active site, prevention of the release of reactive intermediates, substrate recognition, protection of hydrophobic active sites from aggregation, and, in some cases, assistance in the stereospecific binding of the substrate or intermediate to promote efficient catalysis (*4*−*8*). In general, the movement of a flap covering the active site may be either a rigid-body motion with a structural element undergoing rotational and/or translational motion, usually about a hinge, or a structured or flexible element moving to adopt a new stable conformation (*9*). Active site flaps are commonly found in $(\beta/\alpha)_8$-barrel enzymes (*10*) such as triosephosphate isomerase (i.e., TIM[1] barrel), for which structural and catalytic roles of the flap have been studied in considerable detail (e.g., see refs *11*−*20* and references therein), or modified TIM-barrel enzymes such as members of the enolase superfamily, including mandelate racemase (MR) (*2*).

MR (EC 5.1.2.2) from *Pseudomonas putida* catalyzes the Mg^{2+}-dependent 1,1-proton transfer that interconverts the enantiomers of mandelate (Scheme 1) (*21*) and has been studied as a paradigm for understanding enzyme-catalyzed abstraction of a proton from carbon acids (*21*−*25*). Members of the enolase superfamily share a common partial reaction which is the Mg^{2+}-assisted, general base-catalyzed enolization of a carbon acid substrate (*23*, *26*). For example, catalysis by MR proceeds via a two-base mechanism, with His 297 and Lys 166 abstracting the α-proton from (*R*)-mandelate and (*S*)-mandelate, respectively (*1*, *3*, *27*). Although the chemistry for carbon−hydrogen bond cleavage is shared among the members of the enolase superfamily, the enol(ate) intermediate can, depending on the enzyme, subsequently undergo a variety of reactions, including

† This work was supported by a Discovery Grant from the Natural Sciences and Engineering Research Council (NSERC) of Canada.

* To whom correspondence should be addressed. Phone: (902) 494-1974. Fax: (902) 494-1355. E-mail: sbearne@dal.ca.

[1] Abbreviations: BSA, bovine serum albumin; CD, circular dichroism; HEPES, 4-(2-hydroxyethyl)piperazine-1-ethanesulfonic acid; MR, mandelate racemase; 2-NG, 2-naphthylglycolate; TIM, triosephosphate isomerase; VDW, van der Waals.

10.1021/bi7015525 CCC: $40.75
Published on Web 12/20/2007

Scheme 1

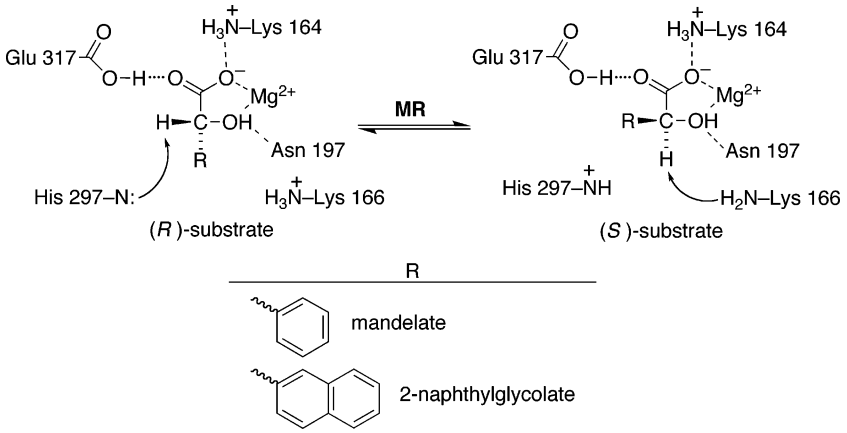

Scheme 2

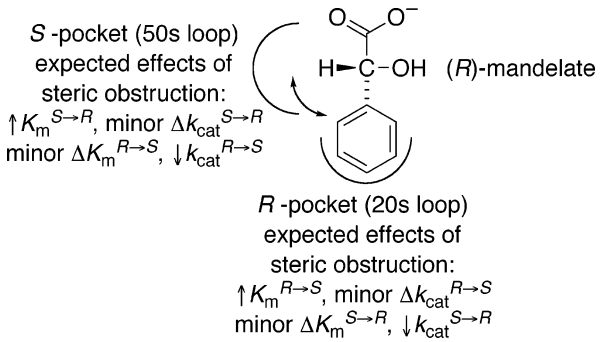

cycloisomerization, β-elimination, epimerization, or racemization as is the case for MR (*26*). Common to the members of the enolase superfamily is a two-domain structure which includes a $(\beta/\alpha)_7$ β-barrel and an N-terminal $\alpha+\beta$ capping domain. Residues located in the 20s and 50s loops of the capping domain are primarily responsible for the substrate specificity (*28*). In MR, these residues comprise the hydrophobic cavity where the phenyl ring of mandelate is bound (*2*). Recently, we proposed that this hydrophobic cavity is partitioned into *R*- and *S*-pockets and that the phenyl group of either (*R*)- or (*S*)-mandelate is bound in its corresponding pocket upon entering the active site (*29*). Since numerous electrostatic interactions appear to anchor the carboxylate and α-hydroxyl functions of the substrate in place, we hypothesized that conversion of the substrate enantiomer into the product enantiomer can only occur if the phenyl group moves during catalysis so that the phenyl group and α-hydrogen exchange positions within the active site. Previously, we tested this hypothesis by examining the effect of replacing Phe 52 and Tyr 54 in the putative *S*-pocket with bulkier tryptophan residues (*29*). The mutant enzymes F52W, Y54W, and F52W/Y54W exhibited a reduction in the level of binding of (*S*)-mandelate relative to (*R*)-mandelate, and a reduction in k_{cat} in the $R \rightarrow S$ direction relative to that observed in the $S \rightarrow R$ direction, consistent with steric obstruction of the *S*-pocket (see Scheme 2) (*29*). The 50s loop was ideally suited for such a study because of its well-defined location within the MR structure. In this work, we complement our previous studies by introducing steric bulk into the putative *R*-pocket using site-directed mutagenesis. Residues that comprise the putative *R*-pocket reside on the 20s loop which is a large, mobile, amphipathic β-meander flap that covers the active site (Figure 1).

There are presently 1260 sequences for members of the enolase superfamily catalyzing 20 different types of reactions with 86 determined X-ray crystal structures (http://sfld.rbvi.ucsf.edu/index.html accessed November 4, 2007) (*30*, *31*). All members of the enolase superfamily have loops of variable size that act as flaps over the active site serving to control access and egress of substrates to and from the active site and to confer substrate specificity (*26*, *28*). Understanding the structure−function relationship for the amino acid residues located in these loops will inform re-engineering of substrate specificity within the enolase superfamily.

A number of elegant mutational studies have been conducted on the active site flap of TIM. These studies have primarily focused on the hinge residues of the flap (*11*−*13*, *15*, *17*, *18*, *32*−*36*), but only limited attention has been devoted to delineating the roles of other residues in the loop (*37*). In addition, the substrate specificity of TIM is limited to the in vivo substrates dihydroxyacetone phosphate and D-glyceraldehyde 3-phosphate [or "parts" thereof (*38*)], making the role of the flap in substrate specificity difficult to study. The less stringent substrate specificity of MR makes this enzyme attractive as a model for studying the effects of loop mutations on substrate specificity.

With the exception of mutations within the putative *S*-pocket (*29*), mutational studies of MR have focused on polar, hydrogen-bonding residues located within or proximal to the active site (*1*, *3*, *39*−*41*). Herein, we describe a detailed study of an enolase superfamily enzyme in which the residues of the flexible loop covering the active site have been mutated in a systematic manner at various sites over the entire loop concomitant with assessment of substrate specificity. A variety of MR mutants were constructed in which the sizes of the hydrophobic side chains of Val 22, Thr 24, Ala 25, Val 26, and Val 29 were varied. Kinetic characterization of these MR mutants using mandelate and the bulkier 2-naphthylglycolate (2-NG) as substrates revealed that MR is quite tolerant of increased steric bulk in the putative *R*-pocket, suggesting that flap mobility may compensate for the variation in the size of the hydrophobic side chains. Indeed, changes in the values of both K_m and k_{cat} were not dramatic, and in general, K_m and k_{cat} were not altered in a manner consistent with selective steric obstruction in the *R*-pocket. Interestingly, a slight increase in the steric bulk of residues located at or near the putative hinge regions of

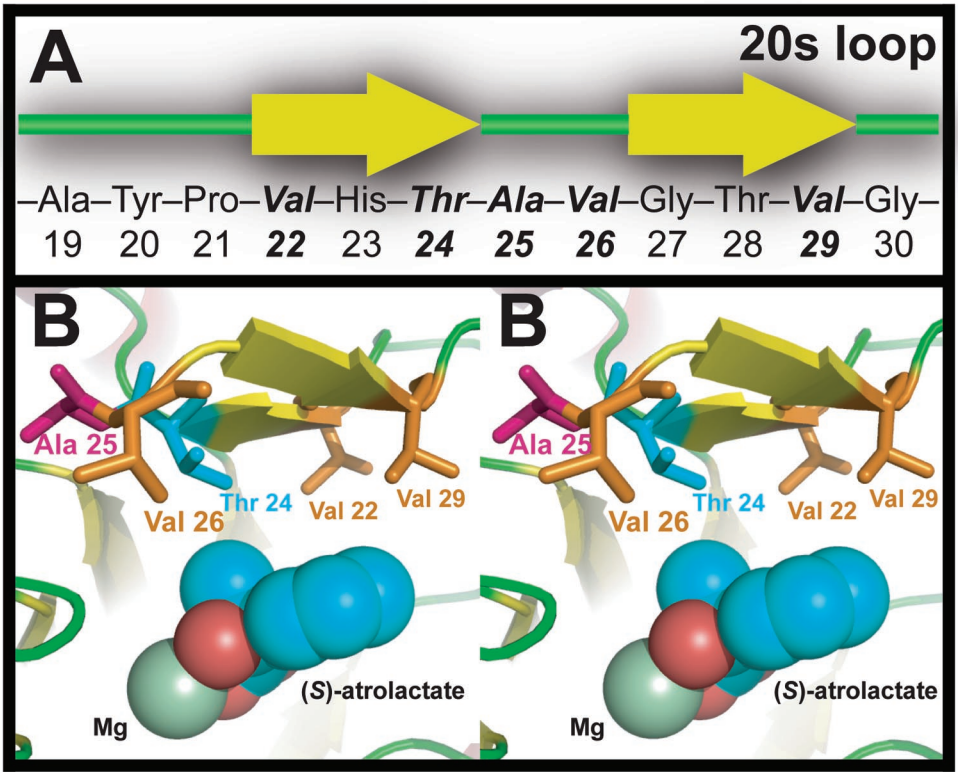

FIGURE 1: Structure of the active site flap. (A) The primary structure of the 20s loop is shown, and the residues mutated in this study are shown in bold italics. (B) The β-meander flap (20s loop) that covers the active site of MR [PDB entry 1MDR (*1*)] is shown in stereoview. The bound substrate analogue (*S*)-atrolactate and the essential Mg^{2+} ion are shown in space-filling representation. The mutated residues are labeled and shown in stick representation. Panel B was prepared using MacPyMol (*99*).

the active site flap altered the substrate specificity to increase the efficiency of racemization of the bulkier substrate 2-NG.

MATERIALS AND METHODS

(*R*)- and (*S*)-mandelic acid, benzohydroxamate, and all other reagents, unless mentioned otherwise, were purchased from Sigma-Aldrich Canada Ltd. (Oakville, ON). (*R*)- and (*S*)-2-naphthylglycolic acid and 2-naphthohydroxamic acid were prepared as described previously (*42*). Deoxyoligonucleotide primers were commercially synthesized by ID Laboratories (London, ON). The QIAprep Spin Miniprep kit (Qiagen Inc., Mississauga, ON) was used for the preparation of plasmids for mutagenesis and transformation. Recombinant MR from *P. putida* was overproduced in and purified from *Escherichia coli* strain BL21(DE3) cells transformed with a pET-15b plasmid (Novagen, Madison, WI) containing the MR open reading frame (ORF) (*41*). This construct encodes the MR gene product with an N-terminal hexahistidine tag [$MGSS(H)_6SSGLVPRGSHM_1$...MR]. The enzyme was purified by metal ion affinity chromatography as described previously (*41*). The hexahistidine tag was not removed from the enzyme since its presence or absence does not influence the kinetic parameters for the recombinant enzyme (*43*). Circular dichroism (CD) assays and spectral measurements were conducted using a JASCO J-810 spectropolarimeter.

Site-Directed Mutagenesis. The pET-15b plasmid bearing the recombinant MR ORF was used as the template for polymerase chain reaction-based site-directed mutagenesis using the QuikChange site-directed mutagenesis kit (Stratagene, La Jolla, CA) and following the protocols described by the manufacturer. The forward (F) and reverse (R) synthetic deoxyoligonucleotide primers used to construct the mutants are listed in Table 1. Potential mutant plasmids were isolated and used to transform competent *E. coli* strain DH5α cells. DH5α cells were used for plasmid maintenance and for all sequencing reactions. Each mutant ORF was sequenced using commercial automated sequencing (Robarts Research Institute, London, ON, or the DalGEN Microbial Genomics Centre DNA Sequencing Facility, Dalhousie University) to ensure that no other alterations of the nucleotide sequence had been introduced. *E. coli* strain BL21(DE3) cells were used as the host for target gene expression.

Enzyme Assays. MR activity was assayed using a CD assay by following the change in ellipticity of mandelate at 262 nm in a quartz cuvette with a 1 cm light path (unless otherwise indicated) as described by Sharp et al. (*44*). All assays were conducted at 25 °C in Na^+-HEPES buffer (0.1 M, pH 7.5) containing $MgCl_2$ (3.3 mM, unless mentioned otherwise) and bovine serum albumin (BSA, 0.005%). The concentrations of (*R*)- and (*S*)-mandelate for assays of all mutant MR enzymes ranged between 0.25 and 10.0 mM. The $MgCl_2$ concentration for all mutants was 3.3 mM, with the exception of V22I and V22I/V29L, which contained 20 mM $MgCl_2$ due to their high K_m^{Mg} values for binding Mg^{2+}. The final concentrations of enzymes used were 150 ng/mL (wild type, V22I, V26A, V29A, and V29L), 231 ng/mL (V22I/V29L), 300 ng/mL (V22A and V22F), 450 ng/mL (T24S, V26L, V26F, and V29F), and 500 ng/mL (A25V and V26A/V29L). For CD-based assays with the substrates (*R*)- and (*S*)-2-NG, the reactions were followed at 266 nm in a quartz cuvette with a 0.1 cm light path

Table 1: Synthetic Deoxyoligonucleotide Primers Used for Site-Directed Mutagenesis

MR mutant	primer type	deoxyoligonucleotide primer[a]
V22A	F	CATTGGCCTACCCCGCTCACACCGCTGTTG
	R	CAACAGCGGTGTGAGCGGGGTAGGCCAATG
V22I[b]	F	CTACCCCATTCACACCGCTGTTGGAACTGT
	R	ACAGTTCCAACAGCGGTGTGAATGGGGTAG
V22F	F	CATTGGCCTACCCCTTCCACACCGCTGTTG
	R	CAACAGCGGTGTGGAAGGGGTAGGCCAATG
T24S	F	GCCTACCCCGTTCACAGCGCTGTTGGAACTGTTGGC
	R	GCCAACAGTTCCAACAGCGCTGTGAACGGGGTAGGC
A25V	F	CCCGTTCACACCGTCGTTGGAACTGTTGGC
	R	GCCAACAGTTCCAACGACGGTGTGAACGGG
V26A	F	CCGTTCACACCGCTGCCGGAACTGTTGGCACAGCGC
	R	GCGCTGTGCCAACAGTTCCGGCAGCGGTGTGAACGG
V26L	F	CCGTTCACACCGCTCTGGGAACTGTTGGCACAGCGC
	R	GCGCTGTGCCAACAGTTCCCAGAGCGGTGTGAACGG
V26F	F	CCGTTCACACCGCTTTCGGAACTGTTGGCACAGCGC
	R	GCGCTGTGCCAACAGTTCCGAAAGCGGTGTGAAGCC
V29A	F	CCGCTGTTGGAACTGCCGGCAGCGCCTCTTGTTTC
	R	GAACAAGAGGCGCTGTGCCGGCAGTTCCAACAGCGG
V29L	F	CCGCTGTTGGAACTCTGGGCACAGCGCCTCTTGTTC
	R	GAACAAGAGGCGCTGTGCCCAGAGTTCCAACAGCGG
V29F	F	CCGCTGTTGGAACTTTCGGCACAGCGCCTCTTGTTC
	R	GAACAAGAGGCGCTGTGCCGAAAGTTCCAACAGCGG
V26A/V29L[c]	F	TTCACACCGCTGCCGGAACTCTGGGCA
	R	TGCCCAGAGTTCCGGCAGCGGTGTGAA
V22I/V29L[c]	F	CCGCTGTTGGAACTCTGGGCACAGCGCCTCTTGTTC
	R	GAACAAGAGGCGCTGTGCCCAGAGTTCCAACAGCGG

[a] All deoxyoligonucleotide sequences are shown in the 5′ → 3′ orientation. The underlined bases designate the codons where mutations were introduced. Both forward (F) and reverse (R) primers are shown. [b] Although the V22L mutant was constructed [5′-CATTGGCCTACCCCCTTCACACCGCTGTTG-3′ (F) and 5′-CAACAGCGGTGTGAAGGGGGTAGGCCAATG-3′ (R)] and its sequence verified by automated DNA sequencing, we were unable to produce the protein. [c] The DNA template used for preparation of all mutants was the pET-15b-MR plasmid, with the exception of V26A/V29L and V22I/V29L for which the templates were the pET-15b-V29L plasmid (the mutated codons for V29L are underlined with dotted lines) and pET-15b-V22I plasmid, respectively.

as described previously (*42*). Reactions were initiated by addition of MR to give the same final enzyme concentration used for assays when mandelate was the substrate. The concentrations of (*R*)- and (*S*)-2-NG for assays of all mutant MR enzymes ranged between 0.10 and 7.5 mM.

Competitive inhibition experiments with 2-naphthohydroxamate were conducted in Na^+-HEPES buffer (0.1 M, pH 7.5) containing $MgCl_2$ (3.3 mM, unless mentioned otherwise) and 20% DMSO as described previously (*42*). The concentrations of (*R*)-mandelate were 0.5, 1.0, 2.0, 5.0, and 10.0 mM. For the V22I and V22I/V29L enzymes (300 ng/mL), the concentrations of 2-naphthohydroxamate were 0, 50.0, 100.0, and 200.0 μM; the concentration of $MgCl_2$ was 20.0 mM. For the V29L enzyme (300 ng/mL), the concentrations of 2-naphthohydroxamate were 0, 12.5, 25.0, and 50.0 μM; the concentration of $MgCl_2$ was 3.3 mM. Inhibition of wild-type MR (150 ng/mL) by 2-naphthohydroxamate (20.0, 40.0, and 60.0 μM) was examined in the presence of 3.3 mM $MgCl_2$ and 20.0 mM $MgCl_2$.

Magnesium Ion Binding. The apparent K_m^{Mg} value for Mg^{2+} was determined for both wild-type and mutant enzymes using the method described by Fee et al. (*45*). Enzyme was first freed of Mg^{2+} by exhaustive dialysis against Na^+-HEPES buffer (0.1 M, pH 8.0) containing EDTA (5 mM), followed by dialysis against Na^+-HEPES buffer (0.1 M, pH 7.5). The enzyme was then incubated with the desired concentration of $MgCl_2$ for 5 min, and then the reaction was initiated by addition of either (*R*)- or (*S*)-mandelate (final concentration, 10 mM). For wild-type MR and all mutant enzymes (with the exception of V22I and V22I/V29L), the concentrations of $MgCl_2$ were 0.05, 0.10, 0.25, 0.50, 1.0, and 2.5 mM. For V22I and V22I/V29L, the concentrations of $MgCl_2$ were 0, 0.25, 0.50, 1.0, 2.5, 5.0, 10.0, 15.0, and 20.0 mM.

Data Analysis and Protein Concentrations. The values of V_{max} and K_m were determined from plots of the initial velocity (v_i) versus substrate concentration ([S]) by fitting the data to eq 1 using nonlinear regression analysis and KaleidaGraph version 3.5 from Synergy Software (Reading, PA). Competitive inhibition constants (K_i) were determined by fitting the initial velocity data to eq 2. The apparent dissociation constant (K_m^{Mg}) for Mg^{2+} was determined from plots of the initial velocity (v_i) versus [Mg^{2+}] by fitting the data to eq 3 using nonlinear regression analysis. All kinetic parameters were determined in triplicate, and average values are reported. The reported errors are standard deviations. Protein concentrations were determined using the Bio-Rad protein assay (Bio-Rad Laboratories, Mississauga, ON) with BSA standards. The values for k_{cat} were calculated by dividing V_{max} values by the total enzyme concentration ($[E]_t$) using the following M_r values: 40 728 Da (wild type), 40 700 Da (V22A, V26A, and V29A), 40 742 Da (V22I, V26L, and V29L), 40 776 Da (V22F, V26F, and V29F), 40 714 Da (V26A/V26L and T24S), and 40 756 Da (A25V and V22I/V29L).

$$v_i = \frac{V_{max}[S]}{K_m + [S]} \quad (1)$$

$$v_i = \frac{V_{max}[S]}{K_m(1 + [I]/K_i) + [S]} \quad (2)$$

$$v_i = \frac{V_{max}[Mg^{2+}]}{K_m^{Mg} + [Mg^{2+}]} \quad (3)$$

Circular Dichroism. The CD spectra for wild-type MR, A25V, and V22I were recorded in sodium phosphate buffer (25 mM, pH 7.5) containing $MgSO_4$ (20 mM) in a quartz cuvette with a 0.1 cm light path over a wavelength range from 195 to 260 nm. Enzyme solutions were dialyzed into sodium phosphate buffer (25 mM, pH 7.5) containing $MgSO_4$ (20 mM), and protein concentrations were determined using the Bio-Rad protein assay with BSA standards in the sodium phosphate buffer. The enzyme concentrations were 63 μg/mL (wild-type MR) and 73 μg/mL (A25V and V22I). CD spectra were analyzed for percent α-helix and β-sheet structure by deconvolution using K2d (*46*).

RESULTS AND DISCUSSION

The "holy grail" of protein engineering is the rational design of enzymes for catalyzing reactions of our choosing under physiological conditions. For example, the ability to rationally design racemases acting on specific substrates would be useful for dynamic kinetic resolutions. Recently, MR-catalyzed racemization, when coupled with the reaction catalyzed by a stereospecific lipase, has been shown to be useful for such resolutions (*47*−*49*). Crystal structures of wild-type and mutant forms of MR complexed with substrate and substrate analogues (*1*, *3*, *39*, *40*) reveal the aromatic ring of all ground state ligands located within a large hydrophobic cavity at the mouth of the enzyme's active site (*2*). This hydrophobic cavity can accommodate a variety of aryl- and heteroaryl-substituted mandelate derivatives that serve as substrates (*50*−*55*). However, the efficiency with which MR catalyzes the racemization of alternative substrates appears to be markedly reduced relative to that exhibited by mandelate. Reengineering the hydrophobic cavity could potentially alter or broaden the substrate repertoire of MR, thereby enhancing the synthetic utility of MR for dynamic kinetic resolutions. However, rational redesign of MR requires a detailed understanding of structure−function relationships in this protein.

Substrate specificity within the enolase superfamily is determined by residues located in the N-terminal capping domain on two loops: the 20s loop and the 50s loop (*28*). A major component of the hydrophobic cavity of the MR active site is the 20s loop which is a large, mobile, amphipathic β-meander flap that extends over the active site as shown in Figure 1 (*2*). Hydrophobic residues within the 20s loop are potentially in van der Waals (VDW) contact with the phenyl group of the substrate during binding and catalysis (*1*, *3*, *39*, *40*). As shown in Figure 1, Val 22 and Val 29 are located at the beginning and end of the β-strands, respectively, near the putative hinge regions where the flap connects to the rest of the N-capping domain.[2] Thr 24, Ala 25, and Val 26 are located at or near the tip of the flap. X-ray crystal structures reveal that the hydroxyl group of the side chain of Thr 24 forms a hydrogen bond across the loop with the backbone carbonyl oxygen of Gly 27 located 2.77 Å away, and the methyl group of the side chain is in VDW contact with ligands (*1*, *3*, *39*, *40*). Ala 25 packs against the rim of the β/α-barrel, thereby "closing" the flap over the active site and excluding bulk solvent.

The structural and dynamic complexity of enzymes often makes it especially difficult to unambiguously interpret the significance of mutagenesis results (*56*). While most of the loop mutations constructed in this work may be regarded as "safe" substitutions (*57*), it is possible that minor structural perturbations of residues that participate in catalysis, substrate binding, exclusion of bulk solvent from the active site, or domain interface interactions could confound interpretation of kinetic results. On the other hand, the flexible nature of the 20s loop may increase the enzyme's "tolerance" for various amino acid substitutions within the loop without any structural perturbations within the β/α-barrel core of the protein.[3] With these caveats in mind, we used site-directed mutagenesis to replace the hydrophobic side chains of several residues in the 20s loop to either reduce or increase the steric bulk of the side chain. Conservative mutations were employed that maintained the hydrophobic character of the side chain but altered the steric bulk, i.e., Ala (92 Å^3) < Val (142 Å^3) < Leu (168 Å^3) ≈ Ile (169 Å^3) < Phe (203 Å^3) (*58*). The effects of the altered steric bulk on MR-catalyzed racemization of mandelate and 2-NG were examined to discern the role of the 20s loop in MR catalysis and substrate specificity.

Magnesium Binding and CD Studies. Site-directed mutagenesis is a valuable tool for exploring the structural and functional importance of particular residues or regions within a protein (*59*), provided that the mutations have a minimal effect on the protein fold and side chain conformations. Because mutation of the flap may perturb the conformation of the enzyme, both the binding of the essential Mg^{2+} and the content of α and β character were measured as an indication of correct folding of the protein (Table 2). Interestingly, replacement of Val 22 with Ile resulted in a 10-fold decrease in the apparent affinity of V22I and V22I/V29L for Mg^{2+}. Consequently, assays with V22I and V22I/V29L were conducted using a $MgCl_2$ concentration of 20 mM (i.e., 5 × apparent K_m^{Mg} for Mg^{2+}) as opposed to 3.3 mM used for the other MR mutants. Mutation of Val 22 caused the most pronounced variation in the apparent affinity

[2] Val 22 and Val 29 are designated as "hinge" residues in this study because of their proximity to nonregular protein structure that precedes and follows the 20s β-meander loop (see Figure 1). X-ray crystal structures of both the liganded (*1*) and unliganded (*2*) forms of MR reveal that the loop is in approximately the same position. Consequently, it is not possible to identify those amino acid residues that might constitute a true hinge.

[3] In addition to mutations having a direct effect on loop structure, dynamics, and solvation, there is the possibility that mutation of the flap might lead to the binding of two substrate molecules. For example, Kallarakal et al. (*3*) observed both (*R*)- and (*S*)-mandelate bound in a sandwich-like arrangement in the X-ray crystal structure of K166R MR. Under initial velocity conditions, it is unlikely that such a complex containing substrate and product would form. Since marked substrate inhibition was not observed for the mutants, it is also unlikely that nonproductive "sandwich" binding of two substrate molecules occurred.

Table 2: Kinetic Parameters for Wild-Type MR and Mutants with Mandelate as the Substrate[a]

	Mg^{2+} affinity	$R \rightarrow S$			$S \rightarrow R$			
	K_m^{Mg} (mM)[b]	K_m (mM)	k_{cat} (s^{-1})	k_{cat}/K_m (M^{-1} s^{-1})	K_m (mM)	k_{cat} (s^{-1})	k_{cat}/K_m (M^{-1} s^{-1})	K_{eq}
wild type	0.34 ± 0.02	1.20 ± 0.04	552 ± 6	(4.6 ± 0.2) × 10^5	0.97 ± 0.09	(4.7 ± 0.1) × 10^2	(4.8 ± 0.3) × 10^5	0.83 ± 0.09
wild type[c]	−	1.47 ± 0.05	(6.2 ± 0.1) × 10^2	(4.3 ± 0.1) × 10^5	1.07 ± 0.04	492 ± 5	(4.6 ± 0.1) × 10^5	0.9 ± 0.2
V22A	0.04 ± 0.01	4.4 ± 0.7	82 ± 3	(1.9 ± 0.2) × 10^4	3.4 ± 0.1	77 ± 2	(2.3 ± 0.1) × 10^4	1.4 ± 0.2
V22I[c]	3.8 ± 0.1	2.9 ± 0.3	(1.15 ± 0.05) × 10^3	(4.0 ± 0.4) × 10^5	1.7 ± 0.3	(7.4 ± 0.1) × 10^2	(4.4 ± 0.7) × 10^5	1.03 ± 0.06
V22F	0.04 ± 0.01	4.4 ± 0.3	98 ± 3	(2.2 ± 0.2) × 10^4	6.1 ± 0.4	98 ± 3	(1.6 ± 0.1) × 10^4	1.0 ± 0.1
T24S	0.29 ± 0.04	2.8 ± 0.2	102 ± 2	(3.7 ± 0.2) × 10^4	3.0 ± 0.1	120 ± 4	(3.6 ± 0.1) × 10^4	1.00 ± 0.09
A25V	0.64 ± 0.02	1.1 ± 0.2	13 ± 1	(1.2 ± 0.1) × 10^4	1.8 ± 0.1	22 ± 1	(1.2 ± 0.1) × 10^4	1.0 ± 0.2
V26A	0.15 ± 0.02	0.91 ± 0.05	304 ± 3	(3.3 ± 0.2) × 10^5	1.7 ± 0.1	550 ± 3	(3.3 ± 0.2) × 10^5	0.9 ± 0.1
V26L	0.12 ± 0.02	1.7 ± 0.1	36 ± 4	(2.1 ± 0.2) × 10^4	1.1 ± 0.2	23 ± 3	(2.1 ± 0.3) × 10^4	1.0 ± 0.2
V26F	0.05 ± 0.02	1.8 ± 0.1	33 ± 1	(1.8 ± 0.1) × 10^4	1.1 ± 0.3	22 ± 2	(2.1 ± 0.3) × 10^4	1.0 ± 0.1
V29A	0.08 ± 0.02	5 ± 1	(2.4 ± 0.2) × 10^2	(4.4 ± 0.4) × 10^4	3.9 ± 0.6	176 ± 4	(4.5 ± 0.6) × 10^4	1.1 ± 0.2
V29L	0.47 ± 0.03	1.7 ± 0.2	(3.0 ± 0.1) × 10^2	(2.6 ± 0.3) × 10^5	0.6 ± 0.1	(1.8 ± 0.1) × 10^2	(2.9 ± 0.3) × 10^5	0.9 ± 0.1
V29F	0.22 ± 0.02	0.9 ± 0.1	53 ± 1	(5.7 ± 0.7) × 10^4	1.1 ± 0.1	53 ± 7	(5.0 ± 0.3) × 10^4	0.8 ± 0.1
V26A/V29L	0.51 ± 0.03	1.4 ± 0.1	106 ± 4	(7.5 ± 0.5) × 10^4	1.1 ± 0.1	89 ± 3	(8.4 ± 0.9) × 10^4	0.96 ± 0.07
V22I/V29L[c]	4.2 ± 0.5	2.8 ± 0.5	(1.01 ± 0.06) × 10^3	(3.7 ± 0.6) × 10^5	1.5 ± 0.1	(7.1 ± 0.2) × 10^2	(4.7 ± 0.4) × 10^5	0.93 ± 0.03

[a] Values are means of triplicate trials, and reported errors are the standard deviations. [b] K_m^{Mg} is the apparent dissociation constant for the MR·Mg^{2+} complex. [c] Kinetic parameters determined using 20 mM Mg^{2+}.

for Mg^{2+} [i.e., K_m^{Mg} values for V22I and V22A (or V22F) differ by 100-fold]. The sensitivity of the apparent affinity for Mg^{2+} to the size of the amino acid side chain at position 22 may arise through variations in the packing interactions with the adjacent Ser 141 which could give rise to subtle changes in conformation that are transmitted from the 131−143 loop to the 167−171 loop and subsequently to Asp 195, one of the Mg^{2+} ligands.

The CD spectra for wild-type MR, A25V, and V22I were recorded between 195 and 260 nm (data not shown), and the secondary structure content was estimated by deconvolution of the CD spectra. A25V was examined because this mutant exhibited the most pronounced decrease in k_{cat}/K_m with respect to mandelate, and V22I was examined because it exhibited the most marked decrease in Mg^{2+} ion binding affinity. Compared with wild-type MR (% α-helix = 38%, % β-sheet = 14%), A25V (30 and 13%, respectively) and V22I (31 and 11%, respectively) did not exhibit a pronounced difference in their α and β content. Although these values are in good agreement with those observed for the X-ray crystal structure of MR complexed with (*S*)-atrolactate (i.e., 40.4 and 19.5%, respectively) (*1*), the presence of minor structural perturbations cannot be ruled out.

Mandelate Racemization. The effects of the flap mutations on the kinetic parameters (Table 2) for mandelate racemization are shown in Figure 2. In terms of substrate binding [for MR, $K_m = K_S$ (*52*)], all mutants exhibited reduced affinity for both (*R*)- and (*S*)-mandelate, with four exceptions (Figure 2A). V29L exhibited a greater affinity for (*S*)-mandelate, while A25V, V26A, and V29F exhibited a greater affinity for (*R*)-mandelate. For hinge residue mutants V22A, V22F, and V29A, which exhibited the greatest reduction in affinity for mandelate, the reduction was only between 4- and 6-fold.

For each of the MR mutants, the rate of turnover (k_{cat}) was reduced between 2- and 42-fold relative to that for wild-type MR, with three exceptions: V22I, V26A, and V22I/V29L (Figure 2B). These latter mutants had k_{cat} values 1.2−2-fold greater than that of wild-type MR. Increasing the steric bulk of the side chains of residues located at or near the tip of the 20s loop (i.e., A25V, V26L, and V26F) caused a 15−42-fold reduction in k_{cat} (vide infra).

Almost all of the mutant enzymes exhibited a decrease in enzyme efficiency (k_{cat}/K_m) with mandelate as the substrate (Figure 2C). Such detrimental effects on catalysis arising from the introduction of a mutation are not surprising considering that MR has evolved to be a "nearly perfect" enzyme (*52*). However, it was surprising that the MR mutants V22I, V26A, and V29L exhibited efficiencies that were very similar to that of wild-type MR. Incorporation of both the V22I and V29L mutations in the double mutant V22I/V29L did not adversely affect the efficiency; however, the presence of both the V26A and V29L mutations in the double mutant V26A/V29L produced an antagonistic effect (*60*), reducing k_{cat}/K_m approximately 6-fold. Thus, for hinge residues 22 and 29, a slight increase in steric bulk (i.e., V22I, V29L, and V22I/V29L) was tolerated quite well, while near the tip of the loop, only a decrease in steric bulk (i.e., V26A) was tolerated. It is not surprising that residues at or near the hinge of an active site flap exhibited some degree of mutability considering the observations reported by Sampson and coworkers who found that a number of sequence solutions at the N-terminal (*18*) and C-terminal (*34*) hinges of the active site flap of TIM gave active enzymes (although amino acid preferences for certain sequence combinations were identified).

Thr 24 was replaced with Ser to remove the γ-methyl group yet retain the intraloop hydrogen bond (*32*, *33*). In this case, a minor reduction in the size of the residue caused a 12-fold decrease in k_{cat}/K_m. This result underscores the potential sensitivity of enzyme catalysis to apparent "minor" changes such as the removal of a single methyl group from an active site flap.

The relatively conservative replacement of Ala 25 with Val at the tip of the loop caused the greatest decrease in k_{cat}/K_m (∼40-fold) of all of the loop mutants examined when mandelate was the substrate, although no significant perturbation in secondary structure was evident from the CD

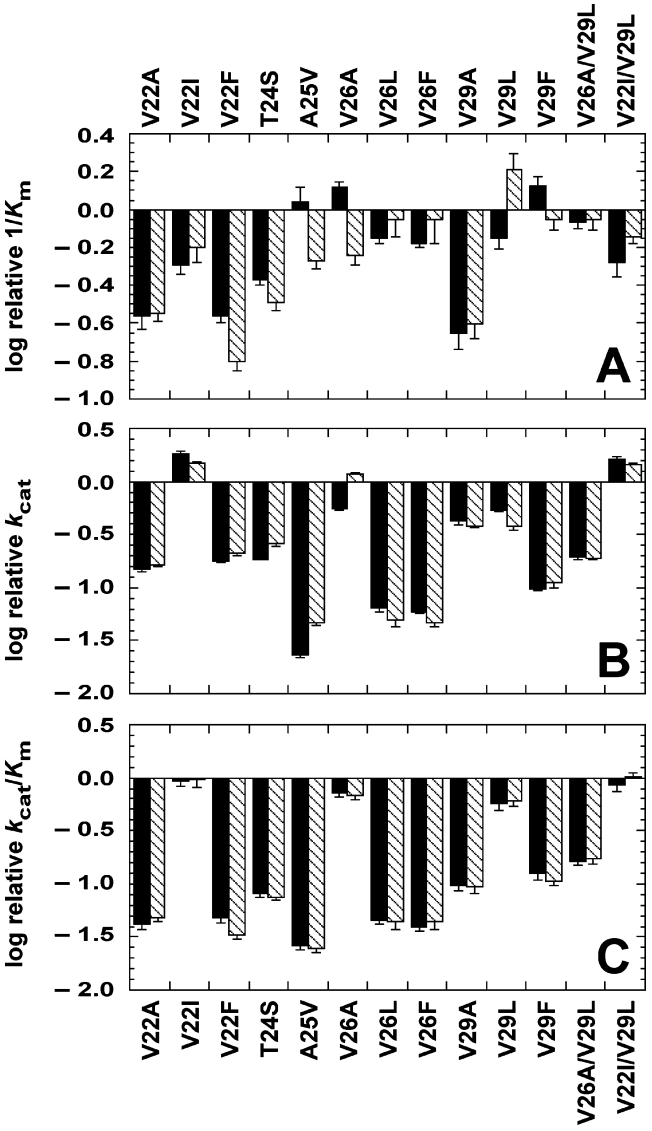

FIGURE 2: Effects of loop mutations on the kinetic parameters for mandelate racemization with reference to the kinetic parameters of wild-type MR. The relative values for mandelate binding (A), turnover (B), and efficiency (C) were calculated using the equations relative $k_{cat} = k_{cat}^{mutant}/k_{cat}^{wild-type}$, relative $1/K_m = K_m^{wild-type}/K_m^{mutant}$, and relative $k_{cat}/K_m = (k_{cat}/K_m)^{mutant}/(k_{cat}/K_m)^{wild-type}$, respectively. Solid bars are for reactions in the $R \rightarrow S$ direction, and hatched bars are for reactions in the $S \rightarrow R$ direction. The average values from three determinations are reported, and the errors shown are the standard deviations.

analysis (vide supra). Hence, MR activity appears to be exquisitely sensitive to the size of this residue located at the tip of the 20s loop. The methyl side chain of Ala 25 packs against Gly 168 and Ser 199 located in loops that form the rim of the β/α-barrel, and our observations suggest that proper packing is critical for catalysis. It appears that Ala 25 is an ideal size to afford stabilization of the altered mandelate in the transition state. VDW interactions between the tip of the loop and the β/α-barrel may be responsible for controlling access to the active site through a highly sensitive gating mechanism similar to the role proposed for a network of weakly polar interactions between the flap tips in the semi-open flap conformation of HIV-1 protease (*61*), or for stabilizing the appropriate flap conformation to exclude bulk solvent from the active site and/or prevent release of the reactive intermediate (e.g., see refs *37*, *62*, and *63*).

The sensitivity of MR to changes in the size of the side chains of Ala 25 and Thr 26 is in contrast to observations on glutathione synthetase from *E. coli* wherein replacement of Gly 229 at the tip of an active site flap with Ala or Val reduced turnover numbers only by approximately 2-fold and had a trivial effect on K_m values (*64*). However, sensitivity of loops to changes in residue size is not unprecedented in the enolase superfamily. For example, Ser 39 of enolase from yeast forms part of the mobile loop that covers the active site and forms a "latch" when chelated to one of the active site Mg^{2+} ions (*65*). Replacement of this residue with Ala caused an 87500-fold reduction in k_{cat}/K_m and an ~10-fold increase in K_m for Mg^{2+} with the emergence of chemistry as the rate-controlling process (*66*, *67*). However, the crystal structure of S39A revealed that the overall fold of the protein was similar to that of the wild-type enzyme with minor differences in conformation confined to the flexible loops near the active site (*67*).

2-NG Racemization. Although MR catalyzes the racemization of the bulky, alternative substrate 2-NG with an efficiency that is ~15-fold lower than that observed for the racemization of mandelate (*42*), 2-NG does serve as an excellent substrate to probe the effect of altered steric bulk within the active site on MR function. The effects of the flap mutations on the kinetic parameters (Table 3) for 2-NG racemization are shown in Figure 3. The pattern for binding the enantiomers of 2-NG by the MR mutants differed from that observed for the binding of mandelate. For many of the mutants, there was an obvious discrimination between the binding of (*R*)- and (*S*)-2-NG, with some of the most pronounced differences being exhibited when a bulky Phe residue was introduced into the *R*-pocket (i.e., V22F, V26F, and V29F).

With the exception of V22I, V29A, and V29L, the values of k_{cat} for all the mutants catalyzing the racemization of 2-NG were reduced between 1.5- and 11-fold in both reaction directions relative to the values observed for wild-type MR (Figure 3B). Most interestingly, the MR mutants with only a *slight* increase in the size of the side chain at the hinge positions, relative to the size of the side chain of valine (i.e., V22I and V29L), had k_{cat} values that were *greater* than those for wild-type MR in both the $R \rightarrow S$ and $S \rightarrow R$ directions. However, these mutations appeared to be antagonistic (*60*) since the value of k_{cat} for V22I/V29L MR was reduced approximately 6-fold in both reaction directions relative to the values observed for wild-type MR. With the exception of V29A, which exhibited k_{cat} values similar to that of wild-type MR, more substantial increases (i.e., V22F and V29F) or decreases (i.e., V22A and V29A) in the steric bulk at positions 22 and 29 caused a reduction in k_{cat} values.

In contrast to the decreased efficiencies resulting from substitution of residues at positions 22, 24−26, and 29 observed when mandelate was the substrate, we were surprised to discover that two of the MR loop mutants were more efficient than wild-type MR at catalyzing the racemization of 2-NG (Figure 3C). V22I and V29L had efficiencies (k_{cat}/K_m) for the racemization of 2-NG that were ~1.6- and ~2.4-fold greater than that of wild-type MR, respectively. While these highly conservative mutations at hinge positions 22 and 29 were tolerated quite well, all other hydrophobic substitutions yielded an approximately 3−13-fold decrease in efficiency, including the V22I/V29L mutant. Similar to

Table 3: Kinetic Parameters for Wild-Type MR and Mutants with 2-NG as the Substrate[a]

	$R \rightarrow S$			$S \rightarrow R$			
	K_m (mM)	k_{cat} (s^{-1})	k_{cat}/K_m (M^{-1} s^{-1})	K_m (mM)	k_{cat} (s^{-1})	k_{cat}/K_m (M^{-1} s^{-1})	K_{eq}
wild type	1.2 ± 0.1	46 ± 1	$(3.8 \pm 0.2) \times 10^4$	1.0 ± 0.2	32 ± 1	$(3.1 \pm 0.1) \times 10^4$	1.1 ± 0.1
wild type[b]	3.5 ± 0.2	70 ± 3	$(2.01 \pm 0.03) \times 10^4$	1.6 ± 0.1	38.4 ± 0.5	$(2.4 \pm 0.1) \times 10^4$	0.97 ± 0.04
V22A	1.9 ± 0.2	15.6 ± 0.3	$(8.1 \pm 0.8) \times 10^3$	1.55 ± 0.03	11.1 ± 0.3	$(7.2 \pm 0.1) \times 10^3$	0.98 ± 0.07
V22I[b]	4.2 ± 0.2	147 ± 2	$(3.4 \pm 0.1) \times 10^4$	2.9 ± 0.1	101 ± 2	$(3.5 \pm 0.1) \times 10^4$	0.9 ± 0.1
V22F	2.2 ± 0.3	10.4 ± 0.6	$(4.7 \pm 0.3) \times 10^3$	0.62 ± 0.05	2.95 ± 0.01	$(4.8 \pm 0.2) \times 10^3$	0.83 ± 0.04
T24S	3.2 ± 0.1	18.3 ± 0.4	$(5.7 \pm 0.2) \times 10^3$	1.4 ± 0.2	8.9 ± 0.4	$(6.6 \pm 0.8) \times 10^3$	0.74 ± 0.07
A25V	1.9 ± 0.1	5.4 ± 0.1	$(2.9 \pm 0.1) \times 10^3$	1.67 ± 0.02	5.8 ± 0.4	$(3.5 \pm 0.1) \times 10^3$	0.9 ± 0.1
V26A	2.1 ± 0.2	30 ± 2	$(1.4 \pm 0.1) \times 10^4$	0.74 ± 0.07	14 ± 1	$(1.9 \pm 0.1) \times 10^4$	0.86 ± 0.08
V26L	1.3 ± 0.1	14 ± 1	$(1.1 \pm 0.1) \times 10^4$	0.62 ± 0.06	8.2 ± 0.2	$(1.3 \pm 0.1) \times 10^4$	0.97 ± 0.09
V26F	1.7 ± 0.2	7.3 ± 0.7	$(4.4 \pm 0.2) \times 10^3$	1.1 ± 0.1	5.4 ± 0.1	$(5.1 \pm 0.4) \times 10^3$	1.05 ± 0.06
V29A	1.8 ± 0.2	53 ± 3	$(3.1 \pm 0.2) \times 10^4$	0.93 ± 0.06	30 ± 1	$(3.2 \pm 0.2) \times 10^4$	0.78 ± 0.07
V29L	1.6 ± 0.1	137 ± 6	$(8.5 \pm 0.2) \times 10^4$	0.80 ± 0.06	65 ± 4	$(8.1 \pm 0.4) \times 10^4$	0.88 ± 0.05
V29F	1.1 ± 0.1	14.1 ± 0.2	$(1.4 \pm 0.1) \times 10^4$	0.55 ± 0.04	9.7 ± 0.4	$(1.8 \pm 0.1) \times 10^4$	1.00 ± 0.05
V26A/V29L	4.4 ± 0.1	23 ± 1	$(5.2 \pm 0.2) \times 10^3$	1.7 ± 0.1	9.8 ± 0.3	$(5.9 \pm 0.2) \times 10^3$	1.23 ± 0.08
V22I/V29L[b]	3.7 ± 0.3	10.5 ± 0.7	$(2.9 \pm 0.1) \times 10^3$	2.4 ± 0.1	7.1 ± 0.1	$(2.9 \pm 0.1) \times 10^3$	0.84 ± 0.04

[a] Values are means of triplicate trials, and reported errors are the standard deviations. [b] Kinetic parameters determined using 20 mM Mg^{2+}.

when mandelate was employed as the substrate, A25V exhibited the largest overall decrease in enzyme efficiency (~13-fold).

For wild-type MR and all mutants examined in this study, the catalytic efficiency was greater when mandelate was the substrate relative to the efficiency when 2-NG was the substrate (Figure 4C). None of the loop mutations, therefore, stabilized the altered 2-NG in the transition state better than they stabilized the transition state for mandelate racemization. All MR mutants exhibited better turnover with mandelate relative to 2-NG (Figure 4B), while they exhibited variability in their affinities for mandelate relative to 2-NG in the ground state (Figure 4A).

With a few exceptions, wild-type and mutant enzymes obeyed the Haldane relationship [i.e., $(k_{cat}/K_m)^{R\rightarrow S}/(k_{cat}/K_m)^{S\rightarrow R} = K_{eq} = 1$ for a racemase] with the calculated equilibrium constants lying within two standard deviations of unity (Tables 2 and 3). The mutants that showed a minor deviation from unity in the Haldane relationship included V22I/V29L with both mandelate and 2-NG as the substrates and V22F, T24S, V29A, V29L, and the two double mutants with 2-NG as the substrate. Although the reason for these deviations is not clear, such deviations have been reported for proline racemase (*68*), mutants of glutamate racemase from *Lactobacillus fermenti* (*69*, *70*), and wild-type glutamate racemases from other organisms (*71*−*73*) and may arise from the enzymes operating via an iso mechanism in which the rate of interconversion of two free enzyme forms differing in protonation state is kinetically significant (*74*).

Putative R-Pocket. Previously, we demonstrated that MR is inhibited by benzilate and, therefore, can simultaneously bind two phenyl rings within its active site (*29*). This led us to hypothesize that the phenyl ring of mandelate may move through the hydrophobic region of the active site between an *R*-pocket and an *S*-pocket during racemization. As an initial test of this hypothesis, we prepared the F52W, Y54W, and F52W/Y54W mutants and demonstrated that the values of k_{cat} and K_m were altered in a manner consistent with steric obstruction of the *S*-pocket (*29*). In the study presented here, we conducted complementary experiments, introducing steric bulk into the putative *R*-pocket. With the exception of Val 29, which appears to interact with the phenyl ring of (*S*)-mandelate in X-ray crystal structures (*1*, *3*, *39*, *40*), much of the putative *R*-pocket is defined by residues 20−26 of the 20s loop. Our expectation was that increasing the steric bulk of residues in the *R*-pocket would increase the value of K_m for (*R*)-mandelate and decrease the value of k_{cat} in the $S \rightarrow R$ direction, relative to the corresponding values for the wild-type enzyme (Scheme 2). However, increasing the sizes of the hydrophobic side chains did not produce any clear trends. Some mutants (i.e., V22I, V26L, V26F, V29L, and V22I/V29L) exhibited a reduced affinity for (*R*)-mandelate relative to (*S*)-mandelate, while other mutants (i.e., V22F, A25V, and V29F) exhibited the opposite enantioselectivity in substrate binding. In addition, increasing the steric bulk in the *R*-pocket did not produce significant discrimination between turnover in either the $S \rightarrow R$ or $R \rightarrow S$ direction (Figure 2). Only for the hinge mutant V29L was the binding of (*R*)-mandelate weaker than that of (*S*)-mandelate and was the value of k_{cat} reduced in the $S \rightarrow R$ direction relative to k_{cat} in the $R \rightarrow S$ direction. However, these differences were not dramatic.

The general insensitivity of the kinetic parameters to the increased steric bulk in the *R*-pocket could have arisen from conformational rearrangement of the 20s loop to compensate for the increased steric hindrance. Therefore, we examined the effect of the mutations on the racemization of 2-NG with the expectation that the kinetic parameters for racemization of this bulkier alternative substrate might be more sensitive to increased steric bulk in the *R*-pocket. Examination of Figure 3A reveals that many of the mutants with increased steric bulk (V22F, V26L, V26F, V29L, V29F, and V26A/V29L) did bind (*R*)-2-NG with an affinity lower than that exhibited for (*S*)-2-NG; however, there were several MR mutants for which a *reduction* in steric bulk within the putative *R*-pocket also caused a reduction in the binding affinity for (*R*)-2-NG (i.e., T24S, V26A, and V29A). In addition, there was not a pronounced reduction in k_{cat} values in the $S \rightarrow R$ reaction direction relative to the $R \rightarrow S$ direction (Figure 3B). V22F is one significant exception to this generalization, exhibiting a 3.5-fold reduction in k_{cat} in the $S \rightarrow R$ direction relative to k_{cat} in the $R \rightarrow S$ direction and a 3.5-fold reduction in the affinity for (*R*)-2-NG relative to (*S*)-2-NG. These observations suggest that Val 22 may play an important role in defining the (*R*)-pocket for the binding of the naphthyl moiety of (*R*)-2-NG. Overall, the effect of

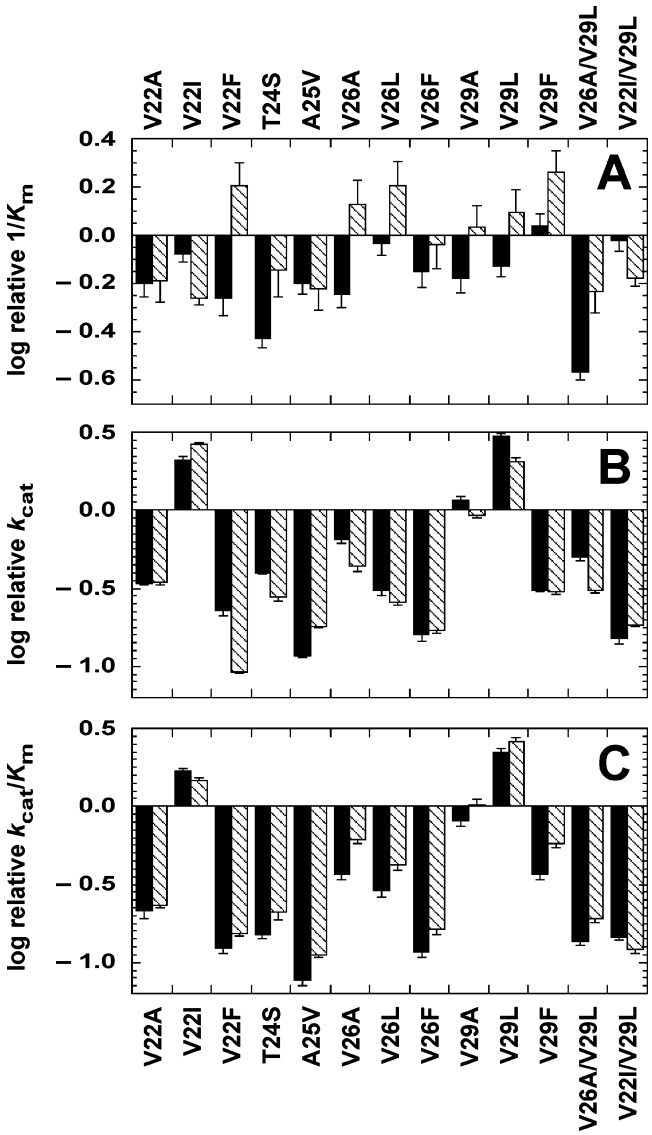

FIGURE 3: Effects of loop mutations on the kinetic parameters for 2-NG racemization with reference to the kinetic parameters of wild-type MR. The relative values for 2-NG binding (A), turnover (B), and efficiency (C) were calculated using the equations relative $k_{cat} = k_{cat}^{mutant}/k_{cat}^{wild-type}$, relative $1/K_m = K_m^{wild-type}/K_m^{mutant}$, and relative $k_{cat}/K_m = (k_{cat}/K_m)^{mutant}/(k_{cat}/K_m)^{wild-type}$, respectively. Solid bars are for reactions in the $R \rightarrow S$ direction, and hatched bars are for reactions in the $S \rightarrow R$ direction. The average values from three determinations are reported, and the errors shown are the standard deviations.

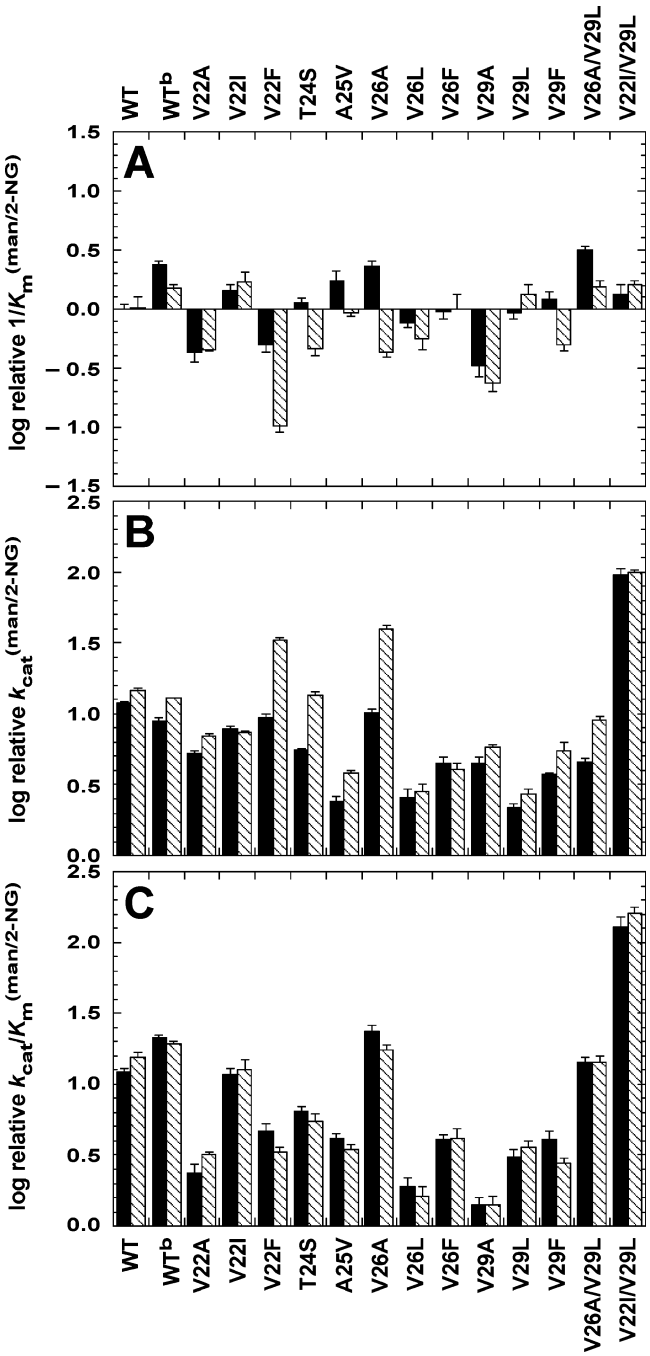

FIGURE 4: Effects of loop mutations on the kinetic parameters for mandelate racemization with reference to the kinetic parameters of 2-NG racemization. For wild-type MR and each mutant, the relative values for mandelate binding (A), turnover (B), and catalytic efficiency (C) were calculated relative to the corresponding values for 2-NG using the equations relative $1/K_m^{man/2-NG} = K_m^{2-NG}/K_m^{man}$, relative $k_{cat}^{man/2-NG} = k_{cat}^{man}/k_{cat}^{2-NG}$, and relative $k_{cat}/K_m^{man/2-NG} = (k_{cat}/K_m)^{man}/(k_{cat}/K_m)^{2-NG}$, respectively. Solid bars are for reactions in the $R \rightarrow S$ direction, and hatched bars are for reactions in the $S \rightarrow R$ direction. The average values from three determinations are reported, and the errors shown are the standard deviations. WT^b indicates that the kinetic parameters for wild-type MR were determined in the presence of 20 mM Mg^{2+}.

increasing steric bulk in the putative *R*-pocket on the kinetic parameters was not as pronounced as we observed when steric obstruction was introduced within the *S*-pocket. This is not surprising considering the more "static" nature of the 50s loop that comprises the *S*-pocket versus the flexible nature of the 20s loop that comprises the *R*-pocket. While these results do not convincingly support our model for motion of the aromatic ring during MR catalysis, they do not rule out the model because it is quite possible that mobility of the flap compensates for increases in the steric bulk of side chains.

Altered Substrate Specificity. The most unexpected finding arising from our mutational analysis of the 20s loop was that a slight increase in steric bulk at either of the hinge positions (22 or 29) resulted in MR mutants that catalyzed the racemization of 2-NG with an efficiency that was ~2-fold greater than that observed for the wild-type enzyme (Figure 3C). This finding was in opposition to our initial expectation that "thinning" the flap by reducing the size of hydrophobic amino acid side chains would enlarge the hydrophobic pocket and lead to more efficient turnover of a bulkier substrate such as 2-NG, which has been observed

Table 4: Competitive Inhibition of Wild-Type and Mutant Mandelate Racemases by 2-Naphthohydroxamate

	K_i (μM)		K_i (μM)
wild type	27 ± 2	V29L	35 ± 7
wild type[a]	23 ± 2	V22I/V29L[a]	112 ± 4
V22I[a]	$(1.9 \pm 0.3) \times 10^2$		

[a] Kinetic parameters determined in the presence of 20 mM Mg^{2+}.

for mutations of active site loops in human carbonic anhydrase II (*75*) and D-hydantoinase (*76*). The enhanced activity arises primarily from an effect on k_{cat}. Since the substrate binding, proton abstraction, and product release steps are all partially rate-limiting for MR catalysis (*52*), the slight increase in steric bulk may stabilize the altered 2-NG in the transition state through direct VDW interactions or alter flap mobility and/or conformation such that the substrate binding and/or product release steps are no longer partially rate-limiting. Our observation that V29L binds the intermediate analogue inhibitor 2-naphthohydroxamate (*42*) with an affinity similar to that exhibited by wild-type MR (see Table 4) suggests that the improved catalytic efficiency of this mutant enzyme for catalyzing the racemization of 2-NG might arise not from its improved ability to bind and stabilize the altered 2-NG in the transition state but due to an effect on the loop. Although one would also expect V22I to exhibit a similar affinity for 2-naphthohydroxamate (at least greater than that exhibited by V22I/V29L), it is possible that the structural perturbations that give rise to the decreased affinity for Mg^{2+} may also adversely affect binding of 2-naphthohydroxamate to V22I and V22I/V29L.

While reengineering an active site flap may imbue an enzyme with new activity (e.g., see refs *77*−*80*), very few studies have focused on modifying the structure of active site flaps to alter or broaden the substrate specificity of enzymes within the enolase superfamily. Gerlt and coworkers found that the efficiency of the *o*-succinylbenzoate synthase activity of the D297G mutant of L-Ala-D/L-Glu epimerase could be increased between 4- and 46-fold through site-directed mutagenesis of Ile 19 in the 20s loop of the epimerase, with residues bearing bulky hydrophobic side chains (e.g., Phe and Tyr) giving some of the largest increases (*28*, *81*). X-ray crystallographic characterization of MR (*2*) and other members of the MR subgroup of the enolase superfamily, including L-fuconate dehydratase (*82*), D-tartrate dehydratase (*83*), and L-talarate/galactarate dehydratase (*84*), as well as the related enzymes D-glucarate dehydratase (*85*, *86*) and D-mannonate dehydratase (*87*) which are archetypes of two new subgroups, has revealed considerable structural and sequence variation in the loop that covers the active site in these enzymes, as might be expected on the basis of their differing substrate specificities. It remains to be tested whether these loops exhibit a similar insensitivity to substitutions as observed for MR.

CONCLUSIONS

While mutation of residues in the 20s loop did not produce striking alterations in the kinetic parameters for the racemization of mandelate that usually accompany mutation of residues such as those that act as general acidic or basic catalysts and are critical for catalysis (*3*, *88*), several trends were evident. (i) Small changes in the size of hydrophobic residues were tolerated reasonably well, and introduction of the bulkier side chain of Phe caused, at most, an ~30-fold reduction in catalytic efficiency, suggesting that flap mobility can compensate for increases in the steric bulk of hydrophobic side chains. (ii) With the exception of V29L, with mandelate as the substrate, and V22F and V26A/V29L, with 2-NG as the substrate, variations in the values of both k_{cat} and K_m revealed that the mutants did not exhibit pronounced enantioselectivity consistent with movement of the aromatic ring during catalysis, perhaps due to flap mobility compensating for the increased size of the hydrophobic side chains. (iii) Residues at the tip of the loop were particularly sensitive to minor alterations in the size of hydrophobic side chains (i.e., T24S and A25V). (iv) A slight increase in the steric bulk of either of the side chains of hinge residue Val 22 or 29 was well-tolerated and favored racemization of the bulkier substrate 2-NG relative to wild-type MR.

Our systematic investigation of the mutability of hydrophobic residues in the active site flap of MR has revealed that alterations of steric bulk have a surprisingly minimal impact on the kinetic constants. This observation suggests that loop flexibility plays an important role in adjustment of the topology of the hydrophobic cavity so that the VDW contacts between the substrate and the nonpolar, non-hydrogen-bonding side chains of the various substituted hydrophobic residues are able to preserve the functional role of the 20s loop (i.e., excluding bulk solvent from the active site and appropriate positioning of the substrate). This structural plasticity is in accord with previous reports of active site plasticity (*89*−*92*) and likely arises because the hydrophobic residues do not have any unique interactions with the substrate. Studies involving the flexible flap of HIV-1 protease have also revealed that mutations of flap residues tend to produce mutants with specificity similar to that of the wild-type enzyme (*93*−*97*). In a recent study of residues located within the active site of glucokinase, Miller (*98*) showed that, while small residues were immutable, the larger amino acid Phe 101 could be replaced by a variety of polar and nonpolar residues of different sizes (e.g., Gly and Trp) with little effect on catalytic activity. This led to the suggestion that non-hydrogen-bonding "shape determinants" might be highly appealing targets for widespread substitution when attempting to alter the catalytic activity of natural enzymes. Our results are in accord with this assertion and indicate that hydrophobic shape determinants residing on a flexible active site flap are quite tolerant of a variety of steric substitutions. However, our results also underscore the inherent difficulties one encounters when redesigning and/or predicting substrate specificity when the substrate binding determinants rely on diffuse hydrophobic or VDW interactions for molecular recognition.

REFERENCES

1. Landro, J. A., Gerlt, J. A., Kozarich, J. W., Koo, C. W., Shah, V. J., Kenyon, G. L., Neidhart, D. J., Fujita, S., and Petsko, G. A. (1994) The role of lysine 166 in the mechanism of mandelate racemase from *Pseudomonas putida*: Mechanistic and crystallographic evidence for stereospecific alkylation by (*R*)-α-phenylglycidate, *Biochemistry 33*, 635−643.
2. Neidhart, D. J., Howell, P. L., Petsko, G. A., Powers, V. M., Li, R. S., Kenyon, G. L., and Gerlt, J. A. (1991) Mechanism of the reaction catalyzed by mandelate racemase. 2. Crystal structure of mandelate racemase at 2.5-Å resolution: Identification of the

active site and possible catalytic residues, *Biochemistry 30*, 9264−9273.
3. Kallarakal, A. T., Mitra, B., Kozarich, J. W., Gerlt, J. A., Clifton, J. G., Petsko, G. A., and Kenyon, G. L. (1995) Mechanism of the reaction catalyzed by mandelate racemase: Structure and mechanistic properties of the K166R mutant, *Biochemistry 34*, 2788−2797.
4. Leszczynski, J. F., and Rose, G. D. (1986) Loops in globular proteins: A novel category of secondary structure, *Science 234*, 849−855.
5. Knowles, J. R. (1991) Enzyme catalysis: Not different, just better, *Nature 350*, 121−124.
6. Kempner, E. S. (1993) Movable lobes and flexible loops in proteins. Structural deformations that control biochemical activity, *FEBS Lett. 326*, 4−10.
7. Gerstein, M., Lesk, A. M., and Chothia, C. (1994) Structural mechanisms for domain movements in proteins, *Biochemistry 33*, 6739−6749.
8. Fetrow, J. S. (1995) Omega loops: Nonregular secondary structures significant in protein function and stability, *FASEB J. 9*, 708−717.
9. Wang, G. P., Cahill, S. M., Liu, X., Girvin, M. E., and Grubmeyer, C. (1999) Motional dynamics of the catalytic loop in OMP synthase, *Biochemistry 38*, 284−295.
10. Wierenga, R. K. (2001) The TIM-barrel fold: A versatile framework for efficient enzymes, *FEBS Lett. 492*, 193−198.
11. Berlow, R. B., Igumenova, T. I., and Loria, J. P. (2007) Value of a hydrogen bond in triosephosphate isomerase loop motion, *Biochemistry 46*, 6001−6010.
12. Kempf, J. G., Jung, J. Y., Ragain, C., Sampson, N. S., and Loria, J. P. (2007) Dynamic requirements for a functional protein hinge, *J. Mol. Biol. 368*, 131−149.
13. Casteleijn, M. G., Alahuhta, M., Groebel, K., El-Sayed, I., Augustyns, K., Lambeir, A. M., Neubauer, P., and Wierenga, R. K. (2006) Functional role of the conserved active site proline of triosephosphate isomerase, *Biochemistry 45*, 15483−15494.
14. Massi, F., Wang, C., and Palmer, A. G. (2006) Solution NMR and computer simulation studies of active site loop motion in triosephosphate isomerase, *Biochemistry 45*, 10787−10794.
15. Eaazhisai, K., Balaram, H., Balaram, P., and Murthy, M. R. N. (2004) Structures of unliganded and inhibitor complexes of W168F, a loop6 hinge mutant of *Plasmodium falciparum* triosephosphate isomerase: Observation of an intermediate position of loop6, *J. Mol. Biol. 343*, 671−684.
16. Kursula, I., Salin, M., Sun, J., Norledge, B. V., Haapalainen, A. M., Sampson, N. S., and Wierenga, R. K. (2004) Understanding protein lids: Structural analysis of active hinge mutants in triosephosphate isomerase, *Protein Eng., Des. Sel. 17*, 375−382.
17. Xiang, J., Jung, J. Y., and Sampson, N. S. (2004) Entropy effects on protein hinges: The reaction catalyzed by triosephosphate isomerase, *Biochemistry 43*, 11436−11445.
18. Xiang, J., Sun, J., and Sampson, N. S. (2001) The importance of hinge sequence for loop function and catalytic activity in the reaction catalyzed by triosephosphate isomerase, *J. Mol. Biol. 307*, 1103−1112.
19. Rozovsky, S., Jogl, G., Tong, L., and McDermott, A. E. (2001) Solution-state NMR investigations of triosephosphate isomerase active site loop motion: Ligand release in relation to active site loop dynamics, *J. Mol. Biol. 310*, 271−280.
20. Rozovsky, S., and McDermott, A. E. (2001) The time scale of the catalytic loop motion in triosephosphate isomerase, *J. Mol. Biol. 310*, 259−270.
21. Gerlt, J. A. (1998) Enzyme-catalyzed proton transfer reactions to and from carbon, in *Bioorganic Chemistry: Peptides and Proteins* (Hecht, S. M., Ed.) pp 279−311, Oxford University Press, New York.
22. Babbitt, P. C., and Gerlt, J. A. (1997) Understanding enzyme superfamilies. Chemistry as the fundamental determinant in the evolution of new catalytic activities, *J. Biol. Chem. 272*, 30591−30594.
23. Babbitt, P. C., Hasson, M. S., Wedekind, J. E., Palmer, D. R., Barrett, W. C., Reed, G. H., Rayment, I., Ringe, D., Kenyon, G. L., and Gerlt, J. A. (1996) The enolase superfamily: A general strategy for enzyme-catalyzed abstraction of the α-protons of carboxylic acids, *Biochemistry 35*, 16489−16501.
24. Gerlt, J. A., Kenyon, G. L., Kozarich, J. W., Neidhart, D. C., and Petsko, G. A. (1992) Mandelate racemase and class-related enzymes, *Curr. Opin. Struct. Biol. 2*, 736−742.
25. Gerlt, J. A., and Gassman, P. G. (1993) Understanding the rates of certain enzyme-catalyzed reactions: Proton abstraction from carbon acids, acyl-transfer reactions, and displacement reactions of phosphodiesters, *Biochemistry 32*, 11943−11952.
26. Gerlt, J. A., Babbitt, P. C., and Rayment, I. (2005) Divergent evolution in the enolase superfamily: The interplay of mechanism and specificity, *Arch. Biochem. Biophys. 433*, 59−70.
27. Powers, V. M., Koo, C. W., Kenyon, G. L., Gerlt, J. A., and Kozarich, J. W. (1991) Mechanism of the reaction catalyzed by mandelate racemase. 1. Chemical and kinetic evidence for a two-base mechanism, *Biochemistry 30*, 9255−9263.
28. Vick, J. E., Schmidt, D. M., and Gerlt, J. A. (2005) Evolutionary potential of $(\beta/\alpha)_8$-barrels: In vitro enhancement of a "new" reaction in the enolase superfamily, *Biochemistry 44*, 11722−11729.
29. Siddiqi, F., Bourque, J. R., Jiang, H., Gardner, M., St. Maurice, M., Blouin, C., and Bearne, S. L. (2005) Perturbing the hydrophobic pocket of mandelate racemase to probe phenyl motion during catalysis, *Biochemistry 44*, 9013−9021.
30. Gerlt, J. A., and Babbitt, P. C. (2001) Divergent evolution of enzymatic function: Mechanistically diverse superfamilies and functionally distinct suprafamilies, *Annu. Rev. Biochem. 70*, 209−246.
31. Babbitt, P. C. (2003) Definitions of enzyme function for the structural genomics era, *Curr. Opin. Chem. Biol. 7*, 230−237.
32. Sampson, N. S., and Knowles, J. R. (1992) Segmental motion in catalysis: Investigation of a hydrogen bond critical for loop closure in the reaction of triosephosphate isomerase, *Biochemistry 31*, 8488−8494.
33. Sampson, N. S., and Knowles, J. R. (1992) Segmental movement: Definition of the structural requirements for loop closure in catalysis by triosephosphate isomerase, *Biochemistry 31*, 8482−8487.
34. Sun, J., and Sampson, N. S. (1998) Determination of the amino acid requirements for a protein hinge in triosephosphate isomerase, *Protein Sci. 7*, 1495−1505.
35. Sun, J., and Sampson, N. S. (1999) Understanding protein lids: Kinetic analysis of active hinge mutants in triosephosphate isomerase, *Biochemistry 38*, 11474−11481.
36. Williams, J. C., and McDermott, A. E. (1995) Dynamics of the flexible loop of triosephosphate isomerase: The loop motion is not ligand gated, *Biochemistry 34*, 8309−8319.
37. Pompliano, D. L., Peyman, A., and Knowles, J. R. (1990) Stabilization of a reaction intermediate as a catalytic device: Definition of the functional role of the flexible loop in triosephosphate isomerase, *Biochemistry 29*, 3186−3194.
38. Amyes, T. L., and Richard, J. P. (2007) Enzymatic catalysis of proton transfer at carbon: Activation of triosephosphate isomerase by phosphite dianion, *Biochemistry 46*, 5841−5854.
39. Mitra, B., Kallarakal, A. T., Kozarich, J. W., Gerlt, J. A., Clifton, J. G., Petsko, G. A., and Kenyon, G. L. (1995) Mechanism of the reaction catalyzed by mandelate racemase: Importance of electrophilic catalysis by glutamic acid 317, *Biochemistry 34*, 2777−2787.
40. Schafer, S. L., Barrett, W. C., Kallarakal, A. T., Mitra, B., Kozarich, J. W., Gerlt, J. A., Clifton, J. G., Petsko, G. A., and Kenyon, G. L. (1996) Mechanism of the reaction catalyzed by mandelate racemase: Structure and mechanistic properties of the D270N mutant, *Biochemistry 35*, 5662−5669.
41. St. Maurice, M., and Bearne, S. L. (2000) Reaction intermediate analogues for mandelate racemase: Interaction between Asn 197 and the α-hydroxyl of the substrate promotes catalysis, *Biochemistry 39*, 13324−13335.
42. St. Maurice, M., and Bearne, S. L. (2004) Hydrophobic nature of the active site of mandelate racemase, *Biochemistry 43*, 2524−2532.
43. Bearne, S. L., St. Maurice, M., and Vaughan, M. D. (1999) An assay for mandelate racemase using high-performance liquid chromatography, *Anal. Biochem. 269*, 332−336.
44. Sharp, T. R., Hegeman, G. D., and Kenyon, G. L. (1979) A direct kinetic assay for mandelate racemase using circular dichroic measurements, *Anal. Biochem. 94*, 329−334.
45. Fee, J. A., Hegeman, G. D., and Kenyon, G. L. (1974) Mandelate racemase from *Pseudomonas putida*. Subunit composition and absolute divalent metal ion requirement, *Biochemistry 13*, 2528−2532.
46. Andrade, M. A., Chacon, P., Merelo, J. J., and Moran, F. (1993) Evaluation of secondary structure of proteins from UV circular

dichroism spectra using an unsupervised learning neural network, *Protein Eng. 6*, 383−390.
47. Felfer, U., Goriup, M., Koegl, M. F., Wagner, U., Larissegger-Schnell, B., Faber, K., and Kroutil, W. (2005) The substrate spectrum of mandelate racemase: Minimum structural requirements for substrates and substrate model, *Adv. Synth. Catal. 347*, 951−961.
48. Larissegger-Schnell, B., Kroutil, W., and Faber, K. (2005) Chemoenzymatic synthesis of (*R*)- and (*S*)-2-hydroxy-4-phenylbutanoic acid via enantio-complementary deracemization of (±)-2-hydroxy-4-phenyl-3-butenoic acid using a racemase-lipase two-enzyme-system, *Synlett 12*, 1936−1938.
49. Strauss, U. T., and Faber, K. (1999) Deracemization of (±)-mandelic acid using a lipase-mandelate racemase two-enzyme system, *Tetrahedron: Asymmetry 10*, 4079−4081.
50. Felfer, U., Strauss, U. T., Kroutil, W., Fabian, W. M. F., and Faber, K. (2001) Substrate spectrum of mandelate racemase: Part 2. (Hetero)-aryl-substituted mandelate derivatives and modulation of activity, *J. Mol. Catal. B: Enzym. 15*, 213−222.
51. Kenyon, G. L., and Hegeman, G. D. (1970) Mandelic acid racemase from *Pseudomonas putida*. Evidence favoring a carbanion intermediate in the mechanism of action, *Biochemistry 9*, 4036−4043.
52. St. Maurice, M., and Bearne, S. L. (2002) Kinetics and thermodynamics of mandelate racemase catalysis, *Biochemistry 41*, 4048−4058.
53. Lin, D. T., Powers, V. M., Reynolds, L. J., Whitman, C. P., Kozarich, J. W., and Kenyon, G. L. (1988) Evidence for the generation of α-carboxy-α-hydroxy-*p*-xylylene from *p*-(bromomethyl)mandelate by mandelate racemase, *J. Am. Chem. Soc. 110*, 323−324.
54. Landro, J. A., Kenyon, G. L., and Kozarich, J. W. (1992) Mechanism-based inactivation of mandelate racemase by propargylglycolate, *Bioorg. Med. Chem. Lett. 2*, 1411−1418.
55. Li, R., Powers, V. M., Kozarich, J. W., and Kenyon, G. L. (1995) Racemization of vinylglycolate catalyzed by mandelate racemase, *J. Org. Chem. 60*, 3347−3351.
56. Fersht, A. (1999) *Structure and Mechanism in Protein Science*, W. H. Freeman and Co., New York.
57. Bordo, D., and Argos, P. (1991) Suggestions for "safe" residue substitutions in site-directed mutagenesis, *J. Mol. Biol. 217*, 721−729.
58. Chothia, C. (1975) Structural invariants in protein folding, *Nature 254*, 304−308.
59. Kraut, D. A., Carroll, K. S., and Herschlag, D. (2003) Challenges in enzyme mechanism and energetics, *Annu. Rev. Biochem. 72*, 517−571.
60. Mildvan, A. S. (2004) Inverse thinking about double mutants of enzymes, *Biochemistry 43*, 14517−14520.
61. Tóth, G., and Borics, A. (2006) Flap opening mechanism of HIV-1 protease, *J. Mol. Graphics Modell. 24*, 465−474.
62. Kato, H., Tanaka, T., Yamaguchi, H., Hara, T., Nishioka, T., Katsube, Y., and Oda, J. (1994) Flexible loop that is novel catalytic machinery in a ligase. Atomic structure and function of the loopless glutathione synthetase, *Biochemistry 33*, 4995−4999.
63. Larson, E. M., Larimer, F. W., and Hartman, F. C. (1995) Mechanistic insights provided by deletion of a flexible loop at the active site of ribulose-1,5-bisphosphate carboxylase/oxygenase, *Biochemistry 34*, 4531−4537.
64. Tanaka, T., Yamaguchi, H., Kato, H., Nishioka, T., Katsube, Y., and Oda, J. (1993) Flexibility impaired by mutations revealed the multifunctional roles of the loop in glutathione synthetase, *Biochemistry 32*, 12398−12404.
65. Wedekind, J. E., Poyner, R. R., Reed, G. H., and Rayment, I. (1994) Chelation of serine 39 to Mg^{2+} latches a gate at the active site of enolase: Structure of the bis(Mg^{2+}) complex of yeast enolase and the intermediate analog phosphonoacetohydroxamate at 2.1-Å resolution, *Biochemistry 33*, 9333−9342.
66. Brewer, J. M., Glover, C. V., Holland, M. J., and Lebioda, L. (1998) Significance of the enzymatic properties of yeast S39A enolase to the catalytic mechanism, *Biochim. Biophys. Acta 1383*, 351−355.
67. Poyner, R. R., Larsen, T. M., Wong, S. W., and Reed, G. H. (2002) Functional and structural changes due to a serine to alanine mutation in the active-site flap of enolase, *Arch. Biochem. Biophys. 401*, 155−163.
68. Fisher, L. M., Albery, W. J., and Knowles, J. R. (1986) Energetics of proline racemase: Racemization of unlabeled proline in the unsaturated, saturated, and oversaturated regimes, *Biochemistry 25*, 2529−2537.
69. Glavas, S., and Tanner, M. E. (2001) Active site residues of glutamate racemase, *Biochemistry 40*, 6199−6204.
70. Glavas, S., and Tanner, M. E. (1999) Catalytic acid/base residues of glutamate racemase, *Biochemistry 38*, 4106−4113.
71. Dodd, D., Reese, J. G., Louer, C. R., Ballard, J. D., Spies, M. A., and Blanke, S. R. (2007) Functional comparison of the two *Bacillus anthracis* glutamate racemases, *J. Bacteriol. 189*, 5265−5275.
72. Lundqvist, T., Fisher, S. L., Kern, G., Folmer, R. H., Xue, Y., Newton, D. T., Keating, T. A., Alm, R. A., and de Jonge, B. L. (2007) Exploitation of structural and regulatory diversity in glutamate racemases, *Nature 447*, 817−822.
73. May, M., Mehboob, S., Mulhearn, D. C., Wang, Z., Yu, H., Thatcher, G. R., Santarsiero, B. D., Johnson, M. E., and Mesecar, A. D. (2007) Structural and functional analysis of two glutamate racemase isozymes from *Bacillus anthracis* and implications for inhibitor design, *J. Mol. Biol. 371*, 1219−1237.
74. Cleland, W. W. (1963) The kinetics of enzyme-catalyzed reactions with two or more substrates or products. I. Nomenclature and rate equations, *Biochim. Biophys. Acta 67*, 104−137.
75. Host, G., Martensson, L. G., and Jonsson, B. H. (2006) Redesign of human carbonic anhydrase II for increased esterase activity and specificity towards esters with long acyl chains, *Biochim. Biophys. Acta 1764*, 1601−1606.
76. Cheon, Y. H., Park, H. S., Kim, J. H., Kim, Y., and Kim, H. S. (2004) Manipulation of the active site loops of D-hydantoinase, a $(\beta/\alpha)_8$-barrel protein, for modulation of the substrate specificity, *Biochemistry 43*, 7413−7420.
77. Suzuki, J., Sasaki, K., Sasao, Y., Hamu, A., Kawasaki, H., Nishiyama, M., Horinouchi, S., and Beppu, T. (1989) Alteration of catalytic properties of chymosin by site-directed mutagenesis, *Protein Eng. 2*, 563−569.
78. Shintani, T., Nomura, K., and Ichishima, E. (1997) Engineering of porcine pepsin. Alteration of S1 substrate specificity of pepsin to those of fungal aspartic proteinases by site-directed mutagenesis, *J. Biol. Chem. 272*, 18855−18861.
79. Okoniewska, M., Tanaka, T., and Yada, R. Y. (1999) The role of the flap residue, threonine 77, in the activation and catalytic activity of pepsin A, *Protein Eng. 12*, 55−61.
80. Wilks, H. M., Moreton, K. M., Halsall, D. J., Hart, K. W., Sessions, R. D., Clarke, A. R., and Holbrook, J. J. (1992) Design of a specific phenyllactate dehydrogenase by peptide loop exchange on the *Bacillus stearothermophilus* lactate dehydrogenase framework, *Biochemistry 31*, 7802−7806.
81. Schmidt, D. M., Mundorff, E. C., Dojka, M., Bermudez, E., Ness, J. E., Govindarajan, S., Babbitt, P. C., Minshull, J., and Gerlt, J. A. (2003) Evolutionary potential of $(\beta/\alpha)_8$-barrels: Functional promiscuity produced by single substitutions in the enolase superfamily, *Biochemistry 42*, 8387−8393.
82. Yew, W. S., Fedorov, A. A., Fedorov, E. V., Rakus, J. F., Pierce, R. W., Almo, S. C., and Gerlt, J. A. (2006) Evolution of enzymatic activities in the enolase superfamily: L-Fuconate dehydratase from *Xanthomonas campestris*, *Biochemistry 45*, 14582−14597.
83. Yew, W. S., Fedorov, A. A., Fedorov, E. V., Wood, B. M., Almo, S. C., and Gerlt, J. A. (2006) Evolution of enzymatic activities in the enolase superfamily: D-Tartrate dehydratase from *Bradyrhizobium japonicum*, *Biochemistry 45*, 14598−14608.
84. Yew, W. S., Fedorov, A. A., Fedorov, E. V., Almo, S. C., and Gerlt, J. A. (2007) Evolution of enzymatic activities in the enolase superfamily: L-Talarate/galactarate dehydratase from *Salmonella typhimurium* LT2, *Biochemistry 46*, 9564−9577.
85. Gulick, A. M., Hubbard, B. K., Gerlt, J. A., and Rayment, I. (2000) Evolution of enzymatic activities in the enolase superfamily: Crystallographic and mutagenesis studies of the reaction catalyzed by D-glucarate dehydratase from *Escherichia coli*, *Biochemistry 39*, 4590−4602.
86. Gulick, A. M., Palmer, D. R., Babbitt, P. C., Gerlt, J. A., and Rayment, I. (1998) Evolution of enzymatic activities in the enolase superfamily: Crystal structure of D-glucarate dehydratase from *Pseudomonas putida*, *Biochemistry 37*, 14358−14368.
87. Rakus, J. F., Fedorov, A. A., Fedorov, E. V., Glasner, M. E., Vick, J. E., Babbitt, P. C., Almo, S. C., and Gerlt, J. A. (2007) Evolution of enzymatic activities in the enolase superfamily: D-Mannonate dehydratase from *Novosphingobium aromaticivorans*, *Biochemistry 46*, 12896−12908.
88. Landro, J. A., Kallarakal, A. T., Ransom, S. C., Gerlt, J. A., Kozarich, J. W., Neidhart, D. J., and Kenyon, G. L. (1991)

Mechanism of the reaction catalyzed by mandelate racemase. 3. Asymmetry in reactions catalyzed by the H297N mutant, *Biochemistry 30*, 9274−9281.
89. Bone, R., Silen, J. L., and Agard, D. A. (1989) Structural plasticity broadens the specificity of an engineered protease, *Nature 339*, 191−195.
90. Aharoni, A., Gaidukov, L., Khersonsky, O., Gould, S. McQ, Roodveldt, C., and Tawfik, D. S. (2005) The 'evolvability' of promiscuous protein functions, *Nat. Genet. 37*, 73−76.
91. Yoshikuni, Y., Ferrin, T. E., and Keasling, J. D. (2006) Designed divergent evolution of enzyme function, *Nature 440*, 1078−1082.
92. Lassila, J. K., Keeffe, J. R., Kast, P., and Mayo, S. L. (2007) Exhaustive mutagenesis of six secondary active-site residues in *Escherichia coli* chorismate mutase shows the importance of hydrophobic side chains and a helix N-capping position for stability and catalysis, *Biochemistry 46*, 6883−6891.
93. Shao, W., Everitt, L., Manchester, M., Loeb, D. D., Hutchison, C. A., and Swanstrom, R. (1997) Sequence requirements of the HIV-1 protease flap region determined by saturation mutagenesis and kinetic analysis of flap mutants, *Proc. Natl. Acad. Sci. U.S.A. 94*, 2243−2248.
94. Tözsér, J., Yin, F. H., Cheng, Y. S., Bagossi, P., Weber, I. T., Harrison, R. W., and Oroszlan, S. (1997) Activity of tethered human immunodeficiency virus 1 protease containing mutations in the flap region of one subunit, *Eur. J. Biochem. 244*, 235−241.
95. Katoh, E., Louis, J. M., Yamazaki, T., Gronenborn, A. M., Torchia, D. A., and Ishima, R. (2003) A solution NMR study of the binding kinetics and the internal dynamics of an HIV-1 protease-substrate complex, *Protein Sci. 12*, 1376−1385.
96. Liu, F., Boross, P. I., Wang, Y. F., Tozser, J., Louis, J. M., Harrison, R. W., and Weber, I. T. (2005) Kinetic, stability, and structural changes in high-resolution crystal structures of HIV-1 protease with drug-resistant mutations L24I, I50V, and G73S, *J. Mol. Biol. 354*, 789−800.
97. Heaslet, H., Rosenfeld, R., Giffin, M., Lin, Y. C., Tam, K., Torbett, B. E., Elder, J. H., McRee, D. E., and Stout, C. D. (2007) Conformational flexibility in the flap domains of ligand-free HIV protease, *Acta Crystallogr. D63*, 866−875.
98. Miller, B. G. (2007) The mutability of enzyme active-site shape determinants, *Protein Sci. 16*, 1965−1968.
99. DeLano, W. L. (2007) *MacPyMOL: A PyMOL-based Molecular Graphics Application for MacOS X*, DeLano Scientific LLC, Palo Alto, CA.

BI7015525